

Incorporation of Metallic Species into Midblock-Sulfonated Block Ionomers

Jing Deng,[§] Jiaqi Yan,[†] Joseph C. Tilly,[†] Liyuan Deng,[§] Kenneth E. Mineart,[¶]
and Richard J. Spontak^{†‡*}

[§]Department of Chemical Engineering, Norwegian University of Science & Technology
7491 Trondheim, Norway

[†]Department of Chemical & Biomolecular Engineering, North Carolina State University
Raleigh, NC 27695, USA

[¶]Department of Chemical Engineering, Bucknell University, Lewisburg, PA 17837, USA

[‡]Department of Materials Science & Engineering, North Carolina State University
Raleigh, NC 27695, USA

(submitted to *Macromolecular Rapid Communications*)

ABSTRACT

Block ionomers can, in the same fashion as their neutral block copolymer analogs, microphase-order into various nanoscale morphologies. The added benefit of a copolymer possessing a charged species is that the resultant block ionomer becomes amphiphilic and capable of imbibing polar liquids, including water. This characteristic facilitates incorporation of metallic species into the soft nanostructure for a wide range of target applications. In this study, we first establish that the nonpolar and polar constituents of solvent-templated midblock-sulfonated block ionomers (SBIs) can be selectively metallated for complementary morphological analysis. Next, four different salts, with cationic charges ranging from +1 to +3, are introduced into three hydrated SBIs varying in their degree of sulfonation (DOS), and cation uptake is measured as a function of immersion time. Our results indicate that uptake generally increases with increasing salt concentration, cationic charge and specimen DOS. Swelling and nanoindentation measurements conducted at ambient temperature demonstrate that water uptake decreases, while the surface modulus increases, with increasing cationic charge. Chemical spectra acquired from energy-dispersive X-ray spectroscopy (EDS) confirm the presence of each of the ion-exchanged species, and corresponding EDS chemical maps reveal that the spatial distribution of these species is relatively uniform throughout the block ionomer films.

* To whom correspondence should be addressed (E-mail: rich_spontak@ncsu.edu)

Introduction

Block copolymers remain one of the most extensively studied classes of macromolecules due to their unique ability to spontaneously self-assemble into a wide variety of soft nanostructures,^[1,2] which makes them especially useful in contemporary technologies.^[3,4] In addition to exhibiting a plethora of morphologies, bicomponent copolymers possessing three or more blocks wherein the endblocks are hard (glassy or semicrystalline) and middle blocks are soft (rubbery) can establish an elastic molecular network.^[5-7] These physically-crosslinked materials, generally classified as thermoplastic elastomers (TPEs),^[8] provide a reusable alternative to chemically-crosslinked elastomers and can be modified through the addition of midblock-selective diluents to generate stimuli-responsive and functional materials (*e.g.*, dielectric elastomers,^[9-11] shape-memory^[12,13] and microfluidics^[14] media, ballistic substrates,^[15] and flexible electronics^[16]). Several independent studies have endeavored to identify the conditions responsible for network formation via midblock bridging^[17-19] and the complex phase behavior^[20,21] of solvated copolymers. While most block copolymers possess neutral charge and are inherently hydrophobic, some copolymers consist of a hydrophilic block (*e.g.*, a polyether), thereby yielding amphiphilic block copolymers. Diblock copolymers of this archetype are often used for surface hydrophilization,^[22-24] whereas triblock copolymers with a hydrophilic midblock are capable of gelling polar species, resulting in technologies ranging from personal care products and pharmaceuticals^[25-28] in the presence of water to gas-separation membranes modified with oligo(ethylene oxide)^[29] and polymer electrolytes^[30-33] with and without ionic liquids.

An alternative approach to introducing hydrophilic moieties into a block copolymer relies on targeting an existing nonpolar block for chemical modification. The seminal studies of Weiss and co-workers^[34,35] are among the first to establish that sulfonation of the styrenic endblocks of

styrenic TPEs possessing an olefinic midblock can yield amphiphilic copolymers. Since, however, the endblocks in this case are hydrophilic, they become plasticized in the presence of a polar solvent and their mechanical properties, required to stabilize the midblock network, are compromised. While several studies of sulfonated triblock copolymers have been reported,^[36-38] only those that are midblock-functionalized^[39-43] are capable of maintaining satisfactory network stability in the presence of a polar medium. A significant commercial advance in this regard is the development of pentablock TPEs composed of poly(*tert*-butylstyrene) endblocks, which are chemically resistant to sulfonation,^[44] poly(ethylene-*alt*-propylene) intermediate blocks for improved mechanical performance and a polystyrene middle block that can be hydrophilized to different levels, as indicated by the degree of sulfonation (DOS). Since the as-cast morphology of these materials solvent-templated from tetrahydrofuran (THF) can be described as a combination of alternating lamellae and styrenic cylinders,^[45] waterborne additives can be readily introduced into the hydrophilic channels or matrix of these sulfonated block ionomers (SBIs) and either ion-exchanged with the protons on the sulfonic acid groups or chemically reduced to form spatially-modulated nanoparticles. The objective of this study is to investigate the introduction of metallic species with different cationic charges into the nanostructure of amphiphilic SBIs.

Experimental

Materials

A homologous series of three poly[*tert*-butylstyrene-*b*-(ethylene-*alt*-propylene)-*b*-(styrene-*co*-styrene sulfonate)-*b*-(ethylene-*alt*-propylene)-*b*-*tert*-butylstyrene] SBI materials depicted in **Figure 1a** and varying in their DOS were provided by Kraton Polymers. Produced by selective sulfonation of a parent pentablock copolymer with corresponding block weights of 15-10-28-10-

15 kDa, they are hereafter designated as SBI n , where n denotes the DOS (in mol%). Lead acetate (Pb[Acetate] $_2$) and ruthenium tetroxide (RuO $_4$) were obtained from Electron Microscopy Sciences, whereas silver nitrate (AgNO $_3$), copper sulfate (CuSO $_4$), zinc chloride (ZnCl $_2$), and aluminum chloride (AlCl $_3$) were all purchased from Sigma-Aldrich. Tetrahydrofuran was supplied by Fisher-Scientific and used as-received.

Methods

Specimen films were prepared by first dissolving each SBI in THF at a concentration of 2% w/v and then casting the resultant SBI/THF solution into a Teflon mold. After drying for 1-2 days at ambient temperature, films measuring \sim 100 μ m thick were immersed in deionized (DI) water under agitation at ambient temperature to remove residual solvent for at least 2 h and subsequently dried in air overnight. Films examined by transmission electron microscopy (TEM) were either immersed in an aqueous solution of Pb[Acetate] $_2$ for 8 h and then vacuum-dried for 12 h prior to cryosectioning, or cryosectioned and then subjected to the vapor of RuO $_4$ (aq) at 500 Pa for 30 min. Images were collected on a JEOL JEM-2200FS microscope operated at 200 kV.

Cation uptake experiments were performed by immersing SBI films into aqueous salt solution at three different concentrations (in M): 0.01, 0.1 and 1.0. Exposure times examined in this work varied from 15 min to 24 h, with the weight of each specimen measured before and after immersion. The experimental cation uptake (n_{exp} , expressed in mmol per gram of polymer) was calculated from $(W_{\text{after}} - W_{\text{before}})/M_c$, where W_{after} and W_{before} represent dry specimen weights after and before ion exchange, respectively, and M_c is the molar mass of the cation in each salt. Trials were repeated at least in quadruplicate to ensure reproducibility. In addition, the theoretical cation uptake (n_{theo}) was determined from the ion exchange capacity (IEC, expressed in meq/g) of each SBI according to $10^{-3}W_{\text{before}}\text{IEC}/q$, where q denotes the charge of a single

electron. According to the manufacturer, the IEC values for SBI26, SBI39 and SBI52 were 1.0, 1.5 and 2.0, respectively. Swelling measurements were conducted in quadruplicate by immersing films after ion exchange into DI water under agitation for 1 h at ambient temperature. Water uptake values were computed from $(W_{\text{wet}} - W_{\text{before}})/W_{\text{before}} \times 100\%$, where W_{wet} constitutes the mass of each hydrated film after careful blotting to remove excess liquid on the film surface.

To discern the presence and distribution of metal species within the ion-exchanged SBI films, back-scattered electron images of uncoated SBI films cryofractured in liquid nitrogen were acquired by variable-pressure scanning electron microscopy (SEM) performed on a Hitachi S3200N instrument operated at 20 kV in the presence of nitrogen at 30 Pa. Associated energy-dispersive X-ray spectroscopy (EDS) yielded both chemical spectra for composition analysis and elemental maps for spatial analysis. Nanoindentation measurements were conducted on a Bruker Hysitron TI980 Triboindenter equipped with a Berkovich diamond tip. The tip area function was determined prior to testing, and a fused quartz standard sample was run prior to testing to ensure instrument accuracy. Two different indentation areas were selected from optical images collected from each sample, and a 5 x 5 array of indentations, spaced 5 μm apart, were performed in each area, yielding a total of 50 indentations per sample. The target indentation depth was 1 μm , and each trial consisted of a 10 s load segment, followed by a 30 s hold segment at the maximum indentation force, and then a final 10 s unload segment. Reduced moduli extracted from the unloading response was corrected for the relevant Poisson's ratios and the tip modulus to yield specimen surface moduli.

Results and Discussion

The TEM images presented in **Figure 1** illustrate how different metal treatments can be used to localize the metal within the microphase-ordered morphologies of SBI52 (**Figure 1b**) and

SBI26 (**Figure 1c**). Both images indicate that the morphologies consist of coexisting lamellae and cylinders. The presence of lamellae in SBI52 is confirmed by three independent methodologies: (i) local curvature analysis of 3D reconstructions generated by transmission electron microtomography,^[45] (ii) small-angle X-ray scattering of specimens as-cast and after solvent-vapor annealing,^[46] and (iii) dissipative particle dynamics simulations.^[46] As with any polymeric system containing styrenic moieties, exposure of SBI52 to the vapor of RuO₄(aq) results in reaction with the phenyl ring and attachment of Ru to the nonpolar microdomains of SBI52, thereby enhancing their electron density (opacity) in **Figure 1b**. While this is particularly useful in identifying the spatial distribution of aromatic moieties in multicomponent (*e.g.*, copolymer or blend) systems for examination by electron microscopy, incorporation of Ru, followed by calcination, can likewise yield surface-functionalized nanoporous materials.^[47] This method of metal modification is not, however, viable from a process standpoint and it is not exclusive to block ionomers. Addition and ion exchange of Pb⁺² from Pb[Acetate]₂ with the sulfonic acid groups in the ionic regions of SBI26 in **Figure 1c** is only possible because those host regions are hydrophilic and permit diffusion of the aqueous solution into the bulk film prior to sectioning. Although modification of any of the SBI materials with Pb is highly beneficial because it allows for unambiguous identification of the spatial location of ionic features, we recognize that such metal incorporation does not serve an immediate purpose.

Ion exchange of various electrolytes using the same methodology, however, provides an attractive route by which to incorporate metal species into SBI52 and its homologs possessing a lower DOS. Ruthenium-based electrolytes that behave as photosensitizers enable these block ionomers to function as both hydrogel^[48,49] and dye-sensitized^[50] organic photovoltaics exhibiting attractive performance metrics, whereas addition of lithium ions can make block

ionomers electroresponsive as an ionic polymer-metal composite.^[51,52] Strategic incorporation of inorganic salts can likewise alter the mechanical properties of these materials.^[53] In this study, we examine the uptake kinetics of four salts varying in cationic charge from +1 to +3 into three different SBI grades at three different solution concentrations. The salts employed for this purpose include Ag(I)NO₃, Cu(II)SO₄, Zn(II)Cl₂, and Al(III)Cl₃, and the aqueous solution concentrations logarithmically range from 0.01 to 1.0 M. The dependence of cation uptake on immersion time is presented (*i*) at different salt concentrations for SBI52 in **Figures 2a-c** and (*ii*) for different SBI grades at 0.1 M salt concentration in **Figures 2d-f**. Results from the first series indicate not only that an increase in salt concentration (particularly from 0.1 to 1.0 M) consistently promotes an increase in cation uptake but also that the Cu and Zn cations with the same +2 charge but different anions yield comparable uptake values (*cf.* **Figure 2b**). While an increase in block ionomer DOS also tends to promote an increase in cation uptake in the second series examined, this effect appears much less distinct due to experimental overlap and uncertainty in the data. To discern the degree of deviation between experimental from theoretical results, we provide these data in the form of $n_{\text{exp}}/n_{\text{theo}}$ for each SBI grade in **Figure S1** in the Supporting Information.

Average cation uptake values are provided as functions of SBI DOS in **Figure 3a** and confirm that uptake is marginally higher in SBI52 than SBI26 and that, except for the Al cation, the uptake in SBI26 is independent of cation within experimental uncertainty. A qualitative assessment made during these experiments is that the films become stiffer after exposure to salt, which is consistent with findings reported elsewhere.^[53] To discern the extent to which such stiffening occurs, we have performed swelling tests (1 h at ambient temperature) on each SBI grade after immersion in 0.1 M aqueous salt solution. In **Figure 3b**, the unmodified control

specimens demonstrate that the extent to which these materials swell decreases by just over half, from ~170% (SBI52) to ~80% (SBI26), as the DOS drops by 50% and the SBI becomes less hydrophilic. Considered relative to **Figure 3a**, the results reported in **Figure 3b** imply that an increase in cation uptake promotes a corresponding reduction in water uptake. This observation is consistent with the expectation that more divalent and trivalent cations would serve to bind more than one sulfonic acid group on the polymer backbone, thereby stiffening the material through physical crosslinking and, as a result, hindering the ability of the hydrophilic microdomains to swell. Moreover, the findings displayed in **Figure 3b** confirm that, irrespective of the cation imbibed, SBI52 with the highest DOS possesses the highest swellability of the SBI series. Addition of the Al cations, in particular, to SBI52 are capable of connecting three sulfonic acid groups/cation, thereby reducing the water uptake by over 400%. As in the case of the cation uptake evident for all species except Al in **Figure 3a**, the extent to which water uptake is lowered in SBI26 appears to be independent of the cation present in **Figure 3b**. Surface moduli measured by nanoindentation are included in **Figure 3c** and likewise verify that the addition of metal cations stiffen SBI52 films subjected to 0.1 M aqueous salt solution for 1 h at ambient temperature. These results are computed from the unloading curve (**Figure S2** in the Supporting Information) and corrected for the Poisson's ratio and modulus of the diamond probe (0.07 and 1140 GPa, respectively⁵⁴) and Poisson's ratio of the SBI (assumed⁵⁵ to be constant at 0.4).

Labeled chemical spectra acquired by EDS confirm the existence of the metal present after immersion of SBI52 in each aqueous salt solution at a concentration of 0.1 M for 24 h. The small peaks for Cu and Zn located just above 8 keV in **Figure 4** correspond to $K\alpha$ X-ray emission lines, whereas the sharper ones in the vicinity of 1 keV are assigned to $L\alpha$ emission lines. Only the $L\alpha$ peaks are visible for Ag (2.98 keV) and Al (1.49 keV). Included (and labeled) in these

spectra are $K\alpha$ peaks for carbon, oxygen and sulfur originating from the block ionomer. The weak and unlabeled $K\alpha$ peak arising from the presence of residual chlorine (from $ZnCl_2$ and $AlCl_3$) at 2.62 keV is slightly higher than the $K\alpha$ peak for sulfur at 2.31 keV. Quantitation of the EDS spectra in **Figure 4** provides the composition of the SBI52 film after metal cation uptake. Measured compositions for Ag, Cu, Zn, and Al are 1.3, 1.1, 1.2, and 2.4 atom%, respectively, and the corresponding S/cation atomic ratios are 1.46, 2.18, 2.00, and 0.67, respectively. As expected from the cation uptake kinetics in **Figure 2** and the water uptake values in **Figure 3b**, incorporation of the trivalent Al yields results that differ substantially from the other three cations, suggesting that this cation interacts differently with the sulfonic acid groups on the SBI52 backbone or perhaps forms complexes on its own.

Cross-sectional SEM images of the same cryofractured SBI52 films from which the EDS spectra have been collected are displayed in **Figure 5** and reveal two important features. The first is that these representative films measure between *ca.* 90 and 160 μm in thickness, according to the SEM images. Secondly, the distribution of Ag is relatively uniform throughout the film, whereas surprisingly large regions appear devoid of metal in films containing the divalent and trivalent cations in the matching EDS elemental maps. While these features might reflect existing topological features (e.g., cracks) evident in the associated SEM images, we propose two nanoscale explanations that could also be responsible for this unexpected observation: (i) large, ordered lamellar regions such as the ones seen in **Figure 1** are prone to defects that can thwart diffusion through ionic pathways, and (ii) divalent and trivalent cations that involve binding to multiple sites within the hydrophilic channels can jam and hinder diffusion. These considerations might also be responsible for the cross-sectional fracture topologies visible in the SEM images. Since the monovalent cations appear uniformly distributed and only the divalent and trivalent

cations display evidence of voids in the EDS maps in **Figure 5**, multiple ionic binding seems to be related to the likely cause, although further analysis is warranted to support this explanation.

Conclusions

Due to their inherently amphiphilic nature, block ionomers continue to find expanding use in a wide range of contemporary technologies. Selective functionalization of the midblock in pentablock copolymers that behave as TPEs yields mechanically robust materials that benefit from the presence of hydrophilic channels or matrices. Incorporation of various metal electrolytes into these regions can endow such materials with beneficial functionality extending from photoresponsiveness to electroactuation. In the present study, we have investigated the uptake kinetics of metal cations varying in charge from +1 to +3 to discern the effects of electrolyte concentration and polymer DOS on cation uptake and metal distribution. The results reported here confirm that the highest levels of uptake occur with the highest valence cation at the highest electrolyte concentration in the SBI with the highest DOS. Addition of the highest valence cation likewise serves to effectively bind the sulfonic acid groups, thereby stiffening the material and reducing swellability. Examination of the chemical make-up of SBI52 films following cation uptake by EDS confirms metal uptake at reasonable levels (except for the high-valence cation), and corresponding elemental maps reveal that the spatial distribution of divalent and trivalent cations in SBI52 is not as uniform as it is for the monovalent cation. These results provide insight into fabrication considerations that can be exploited to introduce metal species into TPE block ionomers for various purposes, such as antibacterial and magnetic properties.

Acknowledgments

We thank the POLYMEM Project (No. 254791) supported by the Norwegian Research

Council, the NC State Nonwovens Institute and Freudenberg Performance Materials for funding. This work was performed in the Analytical Instrumentation Facility (AIF) at North Carolina State University, which is supported by the State of North Carolina and the National Science Foundation (Award No. ECCS-1542015). The AIF is a member of the North Carolina Research Triangle Nanotechnology Network (RTNN), a site in the National Nanotechnology Coordinated Infrastructure (NNCI). We are also grateful to Mr. Phillip Strader for technical assistance.

References

- [1] Abetz, V.; Simon, P. F. W. In *Block Copolymers I* (Ed.: V. Abetz); Springer: Berlin, **2005**.
- [2] Matsen, M. W. *Macromolecules* **2012**, *45*, 2161.
- [3] Bates, C. M.; Bates, F. S. *Macromolecules* **2017**, *50*, 3.
- [4] Müller-Buschbaum, P. (Ed.) *ACS Appl. Mater. Interfaces* **2017**, *9* 31213.
- [5] Flanigan, C. M.; Crosby, A. J.; Shull, K. R. *Macromolecules* **1999**, *32*, 7251.
- [6] Sliozberg, Y. R.; Andzelm, J. W.; Brennan, J. K.; Vanlandingham, M. R.; Pryamitsyn, V.; Ganesan, V. *J. Polym. Sci. B: Polym. Phys.* **2010**, *48*, 15.
- [7] Roos, A.; Creton, C. *Macromolecules* **2005**, *38*, 7807.
- [8] Drobny, J. G. *Handbook of Thermoplastic Elastomers*, 2nd ed.; Elsevier: Oxford, 2014.
- [9] Shankar, R.; Ghosh, T. K.; Spontak, R. J. *Adv. Mater.* **2007**, *19*, 2218.
- [10] Shankar, R.; Ghosh, T. K.; Spontak, R. J. *Soft Matter* **2007**, *3*, 1116.
- [11] Kim, B.; Park, Y. D.; Min, K.; Lee, J. H.; Hwang, S. S.; Hong, S. M.; Kim, B. H.; Kim, S. O.; Koo, C. M. *Adv. Funct. Mater.* **2011**, *21*, 3242.
- [12] Song, S.; Feng, J.; Wu, P. *Macromol. Rapid Commun.* **2011**, *32*, 1569.
- [13] Mineart, K. P.; Tallury, S. S.; Li, T.; Lee, B.; Spontak, R. J. *Ind. Eng. Chem. Res.* **2016**, *55*,

12590.

- [14] Sudarsan, A. P.; Wang, J.; Ugaz, V. M. *Anal. Chem.* **2005**, *77*, 5167.
- [15] Mrozek, R. A.; Leighliter, B.; Gold, C. S.; Beringer, I. R.; Yu, J. H.; VanLandingham, M. R.; Moy, P.; Foster, M. H.; Lenhart, J. L. *J. Mech. Behavior Biomed. Mater.* **2015**, *44*, 109.
- [16] Mineart, K. P.; Lin, Y.; Desai, S. C.; Krishnan, A. S.; Spontak, R. J.; Dickey, M. D. *Soft Matter* **2013**, *9*, 7695.
- [17] Matsen, M. W.; Thompson, R. B. *J. Chem. Phys.* **1999**, *111*, 7139.
- [18] Tallury, S. S.; Spontak, R. J.; Pasquinelli, M. A. *J. Chem. Phys.* **2014**, *141*, 244911.
- [19] Tuhin, M. O.; Woloszczuk, S.; Mineart, K. E.; Pasquinelli, M. A.; Sadler, J. D.; Smith, S. D.; Banaszak, M.; Spontak, R. J. *J. Chem. Phys.*, in press.
- [20] Lodge, T. P.; Pudil, B.; Hanley, K. J. *Macromolecules* **2002**, *35*, 4707.
- [21] Woloszczuk, S.; Tuhin, M. O.; Gade, S. R.; Pasquinelli, M. A.; Banaszak, M.; Spontak, R. *J. ACS Appl. Mater. Interfaces* **2017**, *9*, 39940.
- [22] Alexandridis, P.; Hatton, T. A. *Colloids Interfaces A* **1995**, *96*, 1.
- [23] Kita-Tokarczyk, K.; Junginger, M.; Belegriou, S.; Taubert, A. *Adv. Polym. Sci.* **2011**, *242*, 151.
- [24] Lazzari, M.; Liu, G.; Lecommandoux, S. *Block Copolymers in Nanoscience*; Wiley-VCH: Weinheim, 2006.
- [27] Blanz, A.; Armes, S. P.; Ryan, A. J. *Macromol. Rapid Commun.* **2009**, *30*, 267.
- [28] Shubhra, Q. T. H.; Toth, J.; Gyenis, J.; Feczko, T. *Polym. Rev.* **2014**, *54*, 112.
- [26] Alakhova, D. Y.; Kabanov, A. V. *Mol. Pharm.* **2014**, *11*, 2566.
- [25] Cooksey, T. J.; Singh, A.; Le, K. M.; Wang, S.; Kelley, E. G.; He, L.; Kesava, S. V.; Gomez, E. D.; Kidd, B. E.; Madsen, L. A.; Robertson, M. L. *Macromolecules* **2017**, *50*,

4322.

- [29] Patel, N. P.; Spontak, R. J. *Macromolecules* **2004**, *37*, 2829.
- [30] Elabd, Y. A.; Napadensky, E.; Walker, C. W.; Winey, K. I. *Macromolecules* **2006**, *39*, 399.
- [31] He, Y. Y.; Boswell, P. G.; Buhlmann, P.; Lodge, T. P. *J. Phys. Chem. B* **2007**, *111*, 4645.
- [32] Elabd, Y. A.; Hickner, M. A. *Macromolecules* **2011**, *44*, 1.
- [33] Hallinan, D. T.; Balsara, N. P. *Ann. Rev. Mater. Res.* **2013**, *43*, 503.
- [34] Weiss, R. A.; Sen, A.; Willis, C. L.; Pottick, L. A. *Polymer* **1991**, *32*, 1867.
- [35] Weiss, R. A.; Sen, A.; Pottick, L. A.; Willis, C. L. *Polymer* **1991**, *32*, 2785.
- [36] Wang, Q.; Lu, Y.; Li, N. *Desalination* **2016**, *390*, 33.
- [37] Date, B.; Han, J.; Park, S.; Park, E. J.; Shin, D.; Ryu, C. Y.; Bae, C. *Macromolecules* **2018**, *51*, 1020.
- [38] Escribano, P. G.; del Rio, C.; Morales, E.; Aparicio, M.; Mosa, J. *J. Membr. Sci.* **2018**, *551*, 136.
- [39] Yang, J. C.; Mays, J. W. *Macromolecules* **2002**, *35*, 3433.
- [40] Saito, T.; Moore, H. D.; Hickner, M. A. *Macromolecules* **2010**, *43*, 599.
- [41] Moore, H. D.; Saito, T.; Hickner, M. A. *J. Mater. Chem.* **2010**, *20*, 6316.
- [42] Vargantwar, P. H.; Brannock, M. C.; Tauer, K.; Spontak, R. J. *J. Mater. Chem. A* **2013**, *1*, 3430.
- [43] Choi, J.-H.; Willis, C. L.; Winey, K. I. *J. Membr. Sci.* **2012**, *394-395*, 169.
- [44] Vargantwar, P. H.; Brannock, M. C.; Smith, S. D.; Spontak, R. J. *J. Mater. Chem.* **2012**, *22*, 25262.
- [45] Mineart, K. P.; Jiang, X.; Jinnai, H.; Takahara, A.; Spontak, R. J. *Macromol. Rapid Commun.* **2015**, *36*, 432.

- [46] Mineart, K. P.; Lee, B.; Spontak, R. J. *Macromolecules* **2016**, *49*, 3126.
- [47] Vayer, M.; Nguyen, T. H.; Sinturel, C. *Polymer* **2014**, *55*, 1048.
- [48] Al-Mohsin, H. A.; Mineart, K. P.; Spontak, R. J. *Adv. Energy Mat.* **2015**, *8*, 1401941.
- [49] Al-Mohsin, H. A.; Mineart, K. P.; Armstrong, D. P.; Spontak, R. J. *J. Polym. Sci. B: Polym. Phys.* **2017**, *55*, 85.
- [50] Al-Mohsin, H. A.; Mineart, K. P.; Armstrong, D. P.; El-Shafei, A.; Spontak, R. J. *Sol. RRL* **2018**, 1700145.
- [51] Vargantwar, P. H.; Roskov, K. E.; Ghosh, T. K.; Spontak, R. J. *Macromol. Rapid Commun.* **2012**, *33*, 61.
- [52] Kim, O.; Kim, S. Y. Park, B.; Hwang, W.; Park, M. J. *Macromolecules* **2014**, *47*, 4357.
- [53] Choi, J. H.; Willis, C. L.; Winey, K. I. *J. Membr. Sci.* **2013**, *428*, 516.
- [54] Chowdhury, S.; de Barra, E.; Laugier, M. T. *Surf. Coatings Technol.* **2005**, *193*, 200.
- [55] Bicerano, J. *Prediction of Polymer Properties, 3rd Ed.*; Marcel Dekker: New York, 2009.

List of Figure Captions:

Figure 1. (a) Chemical structure of the SBI materials employed in this study. (b and c) TEM images of (b) SBI52 after exposure to RuO₄(aq) vapor to react with phenyl rings in available nonpolar regions or (c) SBI26 after exposure to Pb[Acetate]₂ to react with sulfonic acid groups in accessible hydrophilic regions. These metal stains result in electron-opaque (dark) features.

Figure 2. Cation uptake presented as a function of immersion time and (a-c) electrolyte concentration (labeled) for SBI52 or (d-f) block ionomer grade (labeled) at 0.1 M electrolyte concentration for four different metal cationic species increasing in charge from left to right. The solid lines serve to connect the data, and the error bars correspond to the standard error.

Figure 3. (a) Average cation uptake values for each of SBI grades examined for four different metal cationic species (labeled). Error bars correspond to the standard deviation. (b) Water uptake measurements for the same SBI grades. Unmodified controls (labeled) are included for comparison, and the error bars denote the standard error. (c) Surface moduli measured by nanoindentation of specimens similar to those prepared for swelling tests. The solid lines serve to connect the data.

Figure 4. EDS chemical spectra acquired from SBI52 after immersion in each 0.1 M electrolyte solution for 1 h. Peaks corresponding to X-ray emission lines from the constituents of the polymer matrix and each incorporated metal are labeled in each spectrum. Details of the peaks are provided in the text. The spectrum for Al has been shifted horizontally by 5 keV to permit incorporation in this layout.

Figure 5. Uncoated SEM images (top row) and EDS elemental maps (bottom row) acquired from each metal anion incorporated into SBI52 under the same experimental conditions as in **Figure 4.**

Figure 1.

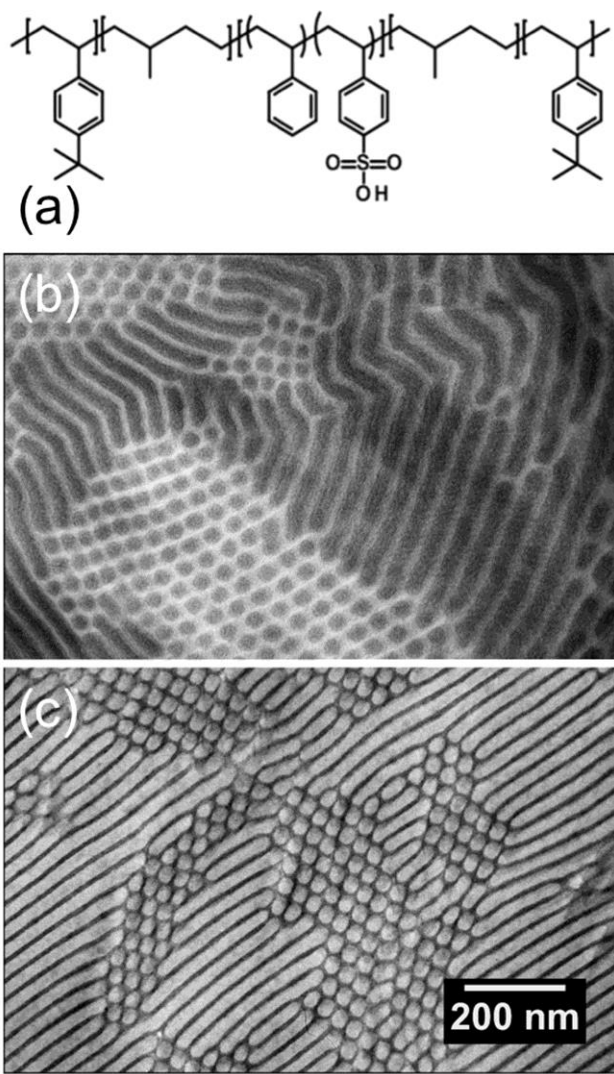


Figure 2.

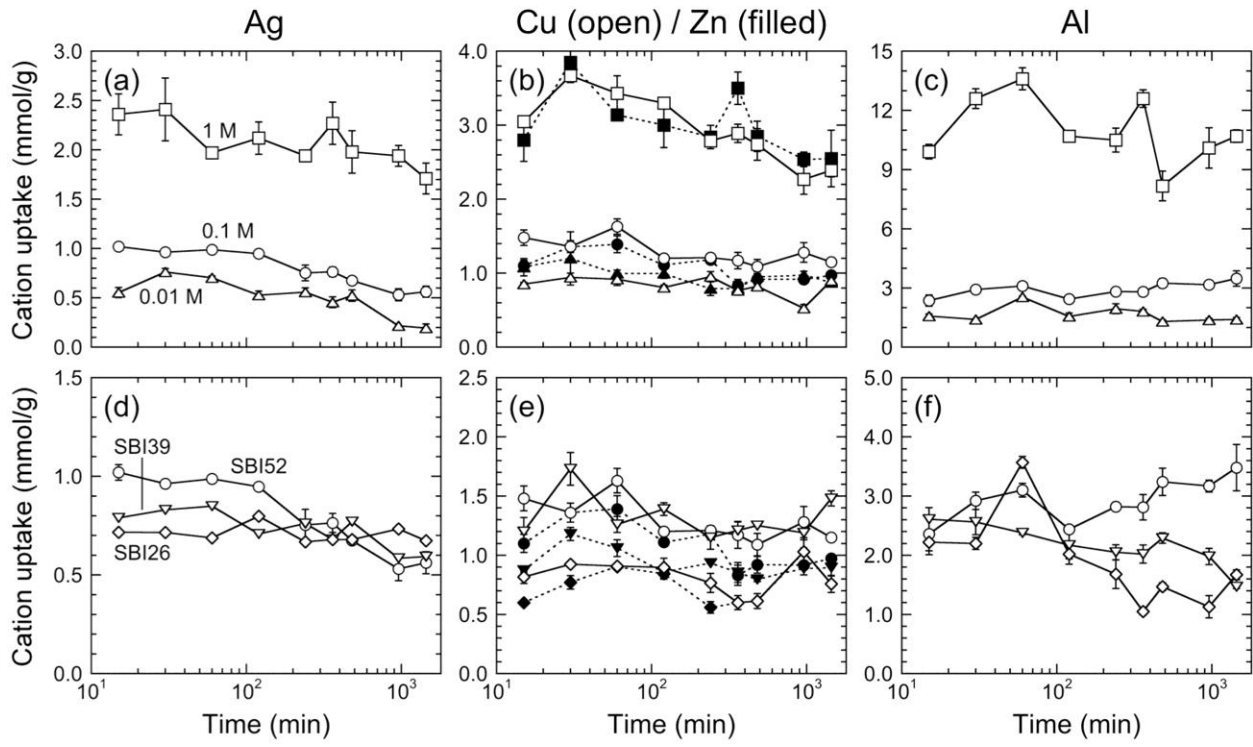


Figure 3.

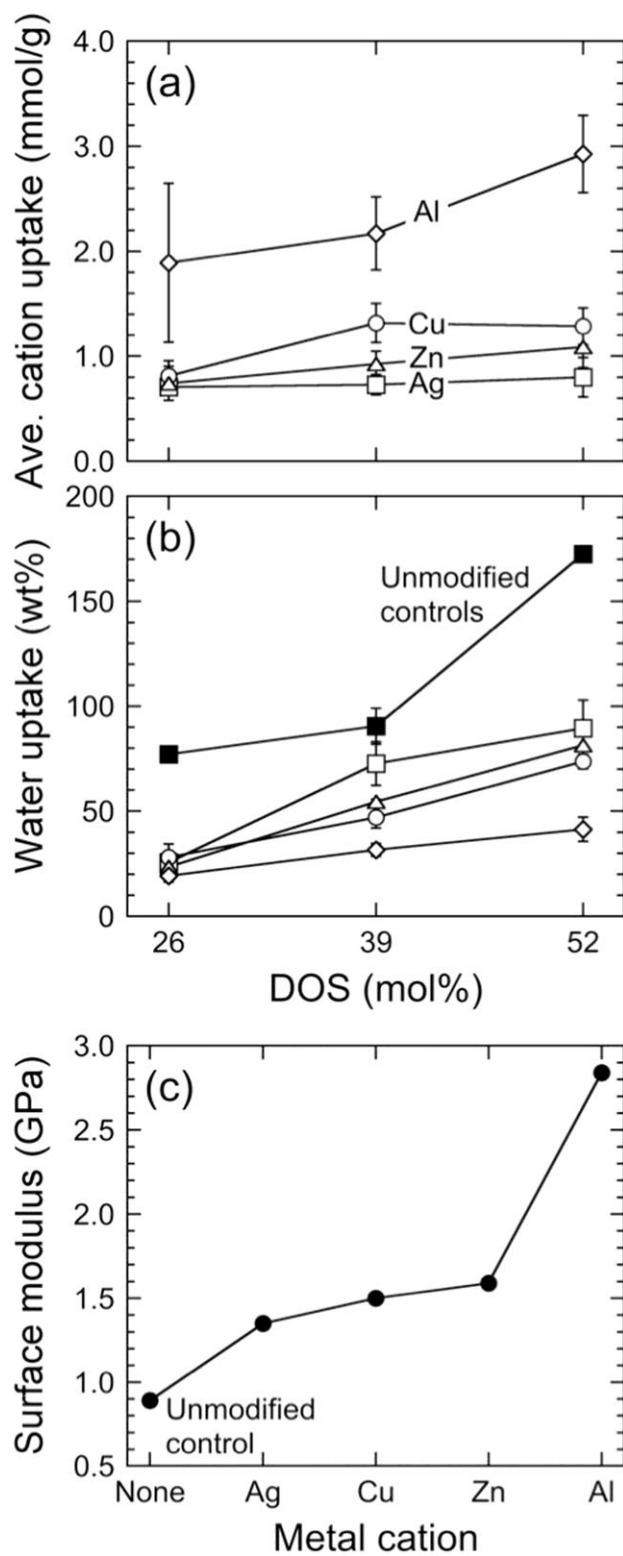


Figure 4.

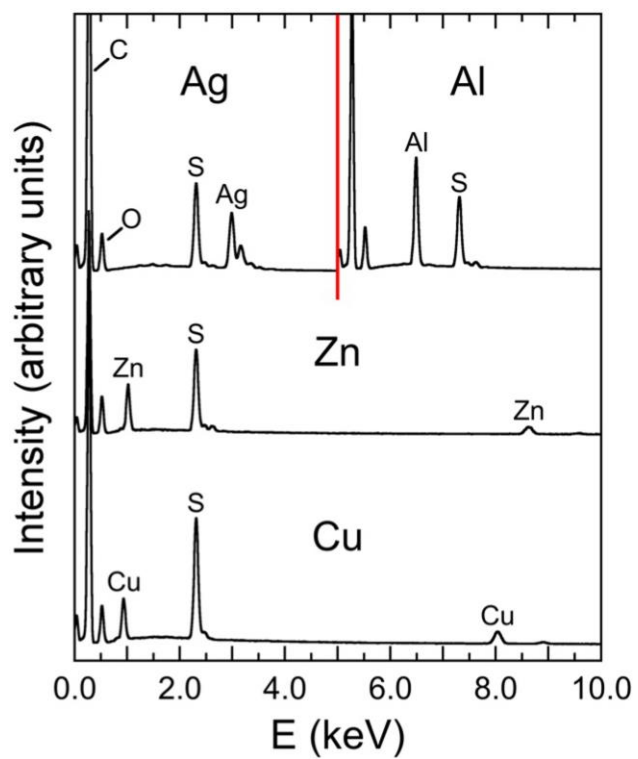


Figure 5.

